

STUDY OF THE EFFECTS OF THERMAL ANNEALING ON SOME SELECTED PROPERTIES OF HETEROJUNCTION PbS-NiO CORE-SHELL THIN FILM

C. AUGUSTINE^{a*}, M. N. NNABUCHI^b, F. N. C. ANYAEGBUNAM^a,
A. N. NWACHUKWU^a

^a*Department of Physics, Federal University Ndufu Alike Ikwo, Ebonyi State*

^b*Department of Industrial Physics, Ebonyi State University, Abakaliki, Ebonyi State*

PbS/NiO core-shell thin film has been synthesized via simple, inexpensive and highly reproducible chemical bath deposition technique and were thermally treated under various annealing temperatures up to 673K in order to determine the effects of thermal annealing on the structural, electrical and optical properties of the film. Our results showed that there is more crystallization and more orientation of the crystal growth with increase in temperature. The variation in conductivity with temperature indicates the semiconducting behaviour of the films suggesting a thermally activated conduction mechanism. The results also revealed that the films show very high absorbance in the UV-VIS regions of the electromagnetic spectrum thereby making the film a very good material for solar thermal applications. The band gap of the thin films is in the range of 1.50 – 1.75eV. The values showing considerably variation with annealing temperatures. The wide range of band gap expands the possibilities of using the thin films for solar photo voltaic application.

(Received January 16, 2017; Accepted May 30, 2017)

Keywords: absorbance, band-gap, thin film, chemical bath, temperature

1. Introduction

Lead sulphide (PbS) is an important direct narrow gap semiconductor material with an approximate energy band gap of 0.4 eV at 300K and a relatively large excitation Bohr radius of 18 nm [1]. It has been widely studied because of its applications in infrared detection [2], photography [3], Pb²⁺ ion selective sensors [4], solar absorption [5] and thin film solar cells [6-8]. In addition, PbS has been utilized as photoresistance, diode lasers, humidity and temperature sensors, decorative and solar control coatings [9-10]. The absorption edge has been found to be red shifted as the particle size increased [11]. These properties have been correlated with the growth conditions and the nature of substrates [12].

Nickel oxide (NiO) is an attractive material because of its chemical stability as well as structural, optical, electrical and magnetic properties. Nickel oxide thin film is a *p*-type semiconducting material with wide band gap of 3.6 - 4 eV, and has cubic rock salt like crystal structure [13-14]. Nickel oxides have been used in different applications like positive electrode in batteries [15], fuel cell [16], solar thermal absorber [17], gas sensors [18], photodetectors [19] and electrochromic devices [20-21]. NiO thin films have useful applications as optically active counter electrodes for window materials and the optical quality of NiO film is improved by annealing [22].

In recent years, the development of core-shell structured materials have been receiving extensive attention because of their various applications such as coatings, solar cells and photocatalysis [23]. The shell can alter the charge, functionality, and reactivity of surface, or improve the stability and dispersive ability. Furthermore, catalytic, optical, or magnetic functions can be imparted to the core particles by the shell material. In general, the synthesis of core/shell structured material has the goal of obtaining a new composite material having synergetic or

* Corresponding author: emmyaustine2003@yahoo.com

complementary behaviours between the core and shell materials [24]. There are many studies on the synthesis of core-shell thin films. Deposition of core-shell thin films by thermal evaporation [25], spin coating [26-27], sputtering [28-30], sol-gel [31-33], chemical vapour deposition [34-36] and chemical bath deposition [24] have been reported. The chemical deposition route is attracting considerable attention as it is relatively inexpensive, simple and convenient for large area deposition. Using chemical deposition method, a number of core-shell, such as ZnO/ TiO₂ and ZnO-Al₂O₃ [37], TiO₂/Fe₂O₃ [38], TiO₂/CoO [39], TiO₂/Cu₂O [40], CdSe/ZnS [41], CdS/ZnO [42], ZnS/ZnO [43] etc. have been reported.

We, in this work, deposited PbS/NiO thin film using Chemical Bath Deposition method. We studied the effects of thermal annealing on the structural, electrical and optical properties of the deposited film.

2. Experimental details

Chemical bath deposition technique was used to deposit heterojunction thin film of PbS/NiO on plane glass substrates in the following order. First, the substrates were degreased in concentrated hydrochloric acid for 24 hours, washed in detergent solutions, rinsed with distilled water and left to dry in dust-free environment. To obtain the deposition of PbS, the chemical bath was composed of 5mls of 0.2M Pb(NO₃)₂, 5mls of 1M SC (NH₂)₂, 5mls of 1M NaOH and 35mls of distilled water put in that order in 50ml cleaned and dried beaker. Five (5) clean glass slides were then inserted vertically into the solution. The deposition was allowed to proceed at room temperature for 50 minutes after which the coated substrates were removed, washed with distilled water and allowed to dry. To obtain the PbS/NiO core-shell, the PbS already formed (core) was inserted in a mixture containing 10mls of 0.2M NiSO₄, 5mls of 100% NH₃ and 27mls of distilled water into 50ml beaker. Deposition was allowed to proceed at temperature of 353K for 1 hr. Two of the deposited films were annealed in an oven at 473K and 673K respectively for 1hr. One of the samples was left unannealed to serve as the control. The X-ray Diffraction (XRD) studies were carried out on the deposited films using the X'PERT-PRO diffractometer which used CuK α radiator of $\lambda = 0.15406\text{nm}$ to scan continuously as 2θ varies from 0 – 100° at a step size of 0.034° and at a scan step time of 57.6s. The ultraviolet-visible (UV-Vis) spectra of the films were measured on UNICO UV-2012 spectrophotometer, in 300-1200 nm wavelength range. The transmission was measured using glass as a reference sample. Four point probes were employed to measure the resistivity of the sample.

3. Results and Discussion

Figs. 1, 2 and 3 show the XRD patterns of PbS/NiO thin films deposited under various thermal treatment. A close look at the three diffractograms show several peaks. Prominent among them are peaks at 2θ values of around 26° and 30° diffraction lines produced by (111) and (200) plane (JCPDS 00-005-0592) respectively. A close look at figures 1-3 shows an improvement in the crystallinity of the films. A comparison between the spectra of the three films show that there is more crystallization and more orientation of the crystal growth in the case of film annealed at 673K. The peaks at 2θ values of 26° and 30° are attributed to Galena PbS (JCPDS 00-005-0592) with lattice parameter $a=5.9362\text{\AA}$. These were assigned to the diffraction line produced by (111) and (200) planes. However, the additional peaks at an angle of 43° and 62° are identified to be NiO (JCPDS 00-047-1049) and are assigned diffraction line produced by (200) and (220) planes of the Bunsenite phase. All these diffraction peaks can be perfectly indexed to cubic crystalline structure. These results suggest that the thin films deposited in this work are mixture of nickel and lead.

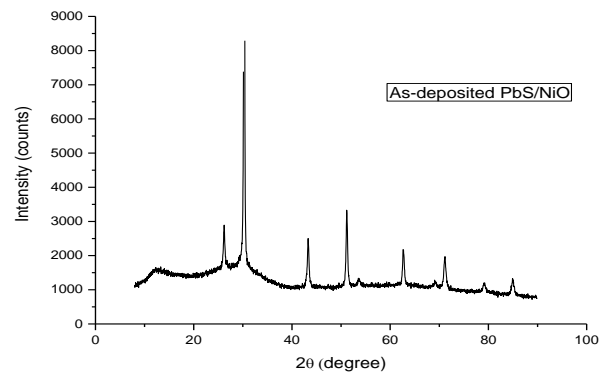


Fig. 1: XRD pattern of PbS/NiO as-deposited

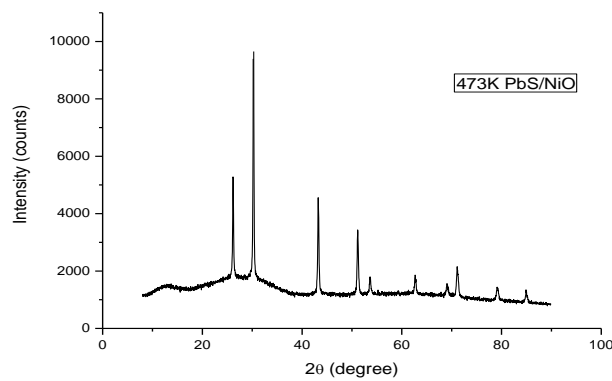


Fig. 2: XRD pattern of PbS/NiO at 473K

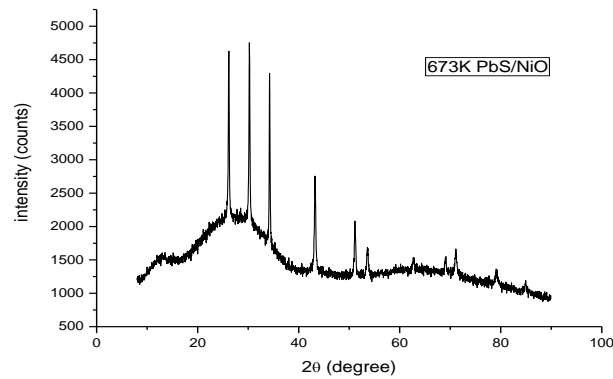


Fig. 3: XRD pattern of PbS/NiO at 673K

The average grain size of the films were calculated using the Scherrer's formula [44].

$$D = \frac{0.9\lambda}{\beta \cos \theta} \quad (1)$$

Where λ is the wavelength of X-rays, β is the full width at half maximum (FWHM) of the peak with the highest intensity and θ is the diffraction angle. The calculated grain size for the annealed film at 473K and 673K are 50.58nm and 58.45nm respectively. The dislocation density, δ and micro strain, μ of the films were calculated using equations (2-3) [45]

$$\delta = \frac{1}{D^2} \quad (2)$$

$$\mu = \frac{\beta \cos \theta}{4} \quad (3)$$

Where D is the crystalline size, β is the full width at half maximum of the peak with the highest intensity and θ is the diffraction angle. δ was estimated as 3.9×10^{14} lines/m² and 2.9×10^{14} lines/m² for thermally annealed 473K and 673K respectively while μ was 0.00011 and 0.00076 respectively.

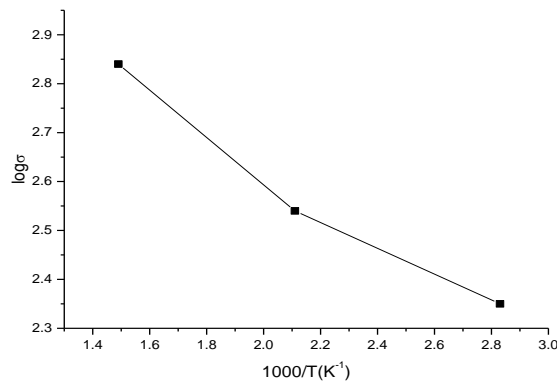


Fig. 4: Variation of electrical conductivity as a function of temperature

The electrical characterization of the PbS/NiO thin films can give a clear idea regarding the transport mechanism related to the electrical conduction which gives the value of electrical resistivity, ρ and conductivity, σ of films. There are various models to explain the conduction process in polycrystalline films based on different scattering mechanisms. The film resistivity, however, may be due to a combination of three mechanisms, namely (1) Due to scattering from phonon impurities and point defects, etc. (2) From film surface, (3) Due to grain boundaries which would be predominant in polycrystalline films. The electrical resistivity, ρ and conductivity, σ were calculated using equations (4-5) [46-47].

$$\rho = 4.52 \left(\frac{V}{I} \right) d \quad (4)$$

$$\sigma = \frac{1}{\rho} \quad (5)$$

Where V is the voltage, I is the current and d is the thin film thickness.

Fig. 4 displays the electrical conductivity, σ versus $1000/T$ curve for as-deposited and thermally annealed 473K and 673K samples. The variation in conductivity with temperature indicates the semiconducting behaviour of the films suggesting a thermally activated conduction mechanism. The thermally annealed 673K film had the highest electrical conductivity. This may be due to the highest grain size of thermally annealed 673K film. The increase of grain size may be due to the improved crystallinity of 673K film. The growth in grains leads to the reduction of grain boundary scattering which decreases the resistivity for the films and eventually the increase in the conductivity of the films [48].

Figs. 5 and 6 are plots of spectral absorbance and transmittance of film samples. From Fig. 5, it is seen that the films display high absorbance in the UV-VIS region dwindling with wavelength in the NIR region with a peak absorbance of 4 which exceeded the maximum of 2 stipulated by Lambert-Beer law [49]. This high value of absorbance recorded by the films may be associated with high concentration of the complexing agent (NH_3) used in precipitating NiO shell on PbS core. At high concentrations, the assumptions of Lambert-Beer law no longer hold [49]. Particle attractive forces come into play at high concentrations, the particles may not act independently of one another so far as absorbing light. Thus, most of the light is absorbed by the particles thereby reducing the transmission of light as it passes through the sample. It is also important to note that PbS alone is a natural absorber in these regions (UV-Vis) [50]. The absorbance decreases exponentially with wavelength for the entire sample annealed at different temperature. A sharp decrease in absorbance was noticed for the entire sample at a wavelength of 800 nm.

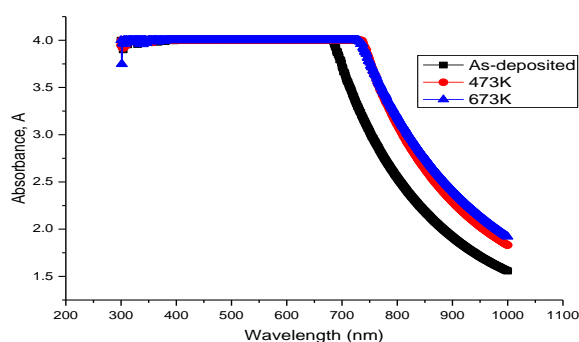


Fig. 5. Absorbance spectra of film samples for as-deposited and annealed at 473K and 673K

Fig. 6 show that the transmittance is generally very low and increases with wavelength for all the film samples. This is due to the increase in crystalline size associated with higher densifications of the film. The plots show that in the NIR region, samples exhibit highest transmittance of about 1.25-3.0% range and virtually zero transmission in the UV-VIS at all temperature. The spectral absorbance and transmittance displayed in Figs, 5 and 6 show that PbS/NiO thin films could be used as spectrally selective coating for solar thermal applications. Solar collectors for heating fluids require increasing the reception area of the solar radiation, and/or to increase the absorbance of the surface coating in order to improve the thermal efficiency.

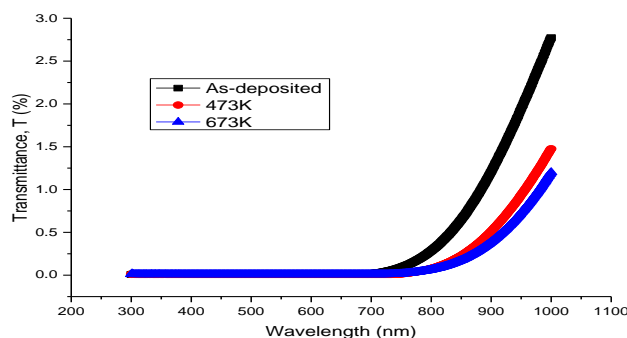


Fig.6. Spectral transmittance of samples for as-deposited and annealed at 473K and 673K

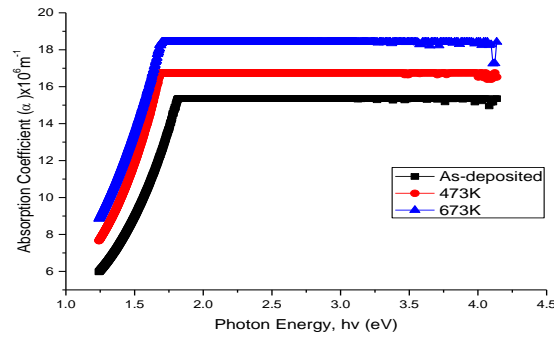


Fig. 7. Plot of α against $h\nu$ of film samples for as-deposited and annealed 473K and 673K

The details of the mathematical determination of the absorption coefficient can be found in literature [51] while the plot of absorption coefficient against photon energy is displayed in Fig.7. The plot of $(\alpha h\nu)^2$ versus $h\nu$ shown in Fig.8 is linear and indicates the presence of direct transition. The straight portion is extrapolated to energy axis at $\alpha = 0$ which gives the band gap energy E_g of the thin film as 1.75eV, 1.65eV and 1.50 eV for the as-deposited, thermally annealed at 473K and 673K respectively. The above suggests that thermal annealing of the samples in oven lowers the values of the band gap. This may be a consequence of the increase in crystalline size associated with high temperature [52]. The energy gap E_g was calculated using the relation:

$$(\alpha h\nu)^2 = A(h\nu - E_g)^n \quad (6)$$

Where A is a constant, $h\nu$ is the photon energy and α is the absorption coefficient. For direct allowed transition, $n = 1/2$ while for indirect ones, $n = 2$ or 3 depending on whether they are allowed or forbidden respectively. Hence a linear graph of $(\alpha h\nu)^2$ versus $h\nu$ will show E_g as intercept on $h\nu$ axis. However, the usual difficulty in applying this concept to polycrystalline thin films with nanometre scale crystalline grain is the size distribution of grains and consistent change in the band gap due to quantum confinement effect [53-54]. Thus the straight line portion may not extend beyond a few tenths of an electron volt and hence value of the band gap could turn out to be very subjective [55].

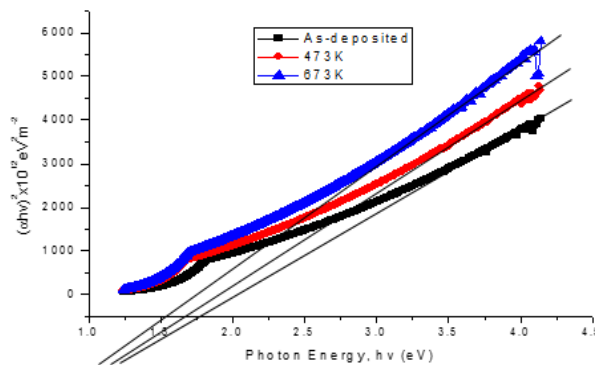


Fig. 8: Plot of $(\alpha h\nu)^2$ as a function $h\nu$ of film samples for as-deposited and annealed at 473K and 673K

The change in energy band gap is given by [44].

$$\Delta E_g = \frac{\hbar^2 v^2}{2R^2} \left(\frac{1}{M_e} + \frac{1}{M_h} \right) - \frac{(1.76e^2)}{\epsilon R} \quad (7)$$

where M_e , M_h are the effective masses of electrons in the conduction band and holes in the valence band respectively, ϵ is the static dielectric constant of the material and ΔE_g is the change in the band gap. The first term represents the particle in a-box quantum localization energy and has an inverse square relation $\frac{1}{R^2}$ dependence where R is the particle radius, while the second term represents the Coulomb energy with $\frac{1}{R}$ dependence. Therefore as R increases due to the increase in the crystalline size associated with temperature annealing, the value of ΔE_g will decrease.

4. Conclusions

Studies of the effects of thermal annealing on the structural, electrical and optical properties of heterojunction PbS/NiO core-shell thin film has been carried out within UV, Visible and NIR regions of electromagnetic spectrum.

The dependence of crystalline size, electrical conductivity and band-gap of the films on the annealing temperatures was particularly investigated. XRD study reveals better crystallization of the films at high temperature, electrical conductivity of the film increases as temperature increases and band-gap analysis show that the band gap of the film decreases as annealing temperature increases. The formation of PbS/NiO heterojunction considerably modified the structural, electrical and optical properties of the independent film.

Acknowledgement

The authors wish to thank the management of Federal University Ndufu Alike Ikwo (FUNAI) for prompt payment of salary which facilitated the completion of the work.

References

- [1] J. L. Machol, F. W. Wise, R. C. Patel, D. B. Tanner, *Phys. Rev. B*, **48**, 2819 (1993).
- [2] P. Gadanne, Y. Yagil, G. Deutscher, *J. Appl. Phys.*, **66**, 3019 (1989).
- [3] P. K. Nair, O. Gomezdaza, M. T. S. Nair, *Adv. Mater. Opt. Electron.*, **1**, 139 (1992).
- [4] H. K. Hirata, B. Higashiyama, *Chem. Soc. Jpn.*, **44**, 2420 (1971).
- [5] T. K. Chaudhuri, S. Chatterjes, *Proceedings of the International Conference on Thermoelectronics*, **11**, 40 (1992).
- [6] P. Nair, *Sol. Energy Mater. Sol. Cells*, **52**, 588 (1998).
- [7] J. J. Valenzuela-Jauregui, R. Ramirez-Bon, G. Mendoza, M. Sotelo-Lerma, *Thin Solid Films*, **104** (2003).
- [8] J. Hernández-Borja, Y. V. Vorobiev, R. Ramírez-Bon, *Sol. Energy Mater. Sol. Cells*, **95**, 1882 (2011).
- [9] P. K. Nair, V. M. Garcia, A. B. Hernandez, M. T. S. Nair, *J. Phys. D: Appl. Phys.*, **24**, 1466 (1991).
- [10] P. Ileana, N. Cristina, I. Violeta, E. Indrea, I. Bratu, *Thin Solid Films* **307**, 240 (1997).

- [11] N. Choudhary, B.K. Sharma, Indian J.Pure. Ap. Phy. **46**, 261 (2008).
- [12] E. Pentia, L. Pintlilie, I. Matei, T. Botila, E. Ozbay, J. Optoelectron. Adv. M. **3**, 525 (2001).
- [13] D. Adler, J. J. Feinleib, Phys. Rev. B, **2**, 3112 (1970).
- [14] M. Zollner, S. Kipp, K. D. Becker, Cryst. Res. Technol. **35**, 299 (2000).
- [15] C. M. Lambert, G. Nazri, P.C. Yu, Sol. Energy Matter. **16**, 1 (1987).
- [16] N. Shaigan, D. G. Ivey, W. Chen, J. Electrochem Soc., **156**, B765 (2009).
- [17] K. R. Cerc, P. Bukovec, B. Pihlar, V. A. Sureau, B. Orel, G. Drazie, Solid State Ionics **165**, 191 (2003).
- [18] I.Hotovy, J. Huran, L. Spiess, R. Capkovic, S.Hascik, Vacuum **58**(2-3), 300 (2000).
- [19] M. C. Leong, I. M. Seongil, Applied Surface Science, **244**(1-4), 435 (2005).
- [20] K. K. Purushothaman, G. Muralidharan, J.Sol-Gel Sci. Technol. **46**, 190 (2008).
- [21] F. F. Ferreira, M. H. Tabacniks, M. C. A. Fantini, I.C. Faria, A. Gorenstein, Solid State Ionics. **86**, 971 (1996).
- [22] P. Vikas, P. Shailesh, C. Manik, G. Prasad, S. Ratnakar, S. Shashwat, J. Pradeep, Journal of Surface Engineered Materials and Advanced Technology **1**, 35 (2011).
- [23] D. U. Onah, C. E. Okeke, F. I. Ezema, A. B. C. Ekwealor, R. U. Osuji, B. A. Ezekoye, Journal of Ovonic Research, **8**(5), 105 (2012).
- [24] P. E. Agbo, M. N. Nnabuchi, Chalcogenide Letters, **8**(4), 273 (2011).
- [25] M. A. Manal, H. H. Noor, I. M. Hanaa, H. M. Ghuson, A. A. Kadhim, F. A. Ameer. Journal of Electron Devices, **12**, 761 (2012).
- [26] L. Hung-Ju, Study and applications of hybrid organic/inorganic semiconductor quantum dots in thin films, PhD Thesis, National Central University, Taiwan in Science and Aix-Marseille University, France, (2014).
- [27] H. Y. Liang, H. G. Zhao, Z. P. Li, C. Harnagea, D. L. Ma, Silver Nanoparticle film induced Photoluminescence Enhancement of Near-infrared Emitting PbS and PbS/CdS Core/Shell Quantum Dots: Observation of Different Enhancement Mechanisms, Royal Society Chemistry, (2016).
- [28] S. M. John, J. Weilin, C. D. Timothy, V. Tamas, K. Libor, Journal of Applied Physics **14**(8), 10 (2013).
- [29] S. Xiao-Jing, M. Shu-Yi, W. Jin-Jun, X. Xiao-Li, National Center for Biotechnology Information, USA **28** (9), 2033 (2008)..
- [30] C. Yu-lun, H. Chin-Hua, C. Mu-Tung, C. Li-Jen, S. L. Chang, H. S. Jin, G. Jun-Yiew, L. W. Zhong, (2006). RuO₂ Nanowires and RuO₂/TiO₂ core-shell Nanowires: From synthesis to Mechanical, Optical, Electrical and Photoconductive Properties, Advanced Materials.
- [31] J. Zhang, Z. Liu, B. Han, Z. Li, G. Yang, J. Li, J. Chen, Journal of Supercritical Fluids **36** (3) 194 (2006).
- [32] T. Y. Wei, B. M. Sanchez, P. J. Dobson, P. S. Grant, Adv. Mater. **22**, 347 (2010).
- [33] O. Sadek, S. Reda, R. Al-Bilali, Advances in Nanoparticles **2**, 165 (2013).
- [34] L. Yuwei, C. Wei-Jen, Y. L. Jiun, H. C. Yuan, L. Chi-Te, F. C. Yang, L. Jing-Yu, Nanoscale Research Letters, **7**(1), 401 (2012)..
- [35] N. F. B. Nazarudin, S. N. Azizan, S. A. Rahman, B. T. Goh, Growth and Structural property Studies on NiSi/SiC core-shell nanowires by hot-wire chemical vapour deposition, (2014).
- [36] L. F. Cui, Y. Yang, C. M. Hsu, Y. Cui, Nano Letter **9**(9), 3370 (2009).
- [37] L. Matt, E. G. Lori, R. Aleksandra, K. Teoye, L. Jan, Y. Peideng, J. Phys. Chem, pp. 22652. (2006).
- [38] P. E. Agbo, M. N. Nnabuchi, D. U. Onah, Journal of Ovonic Research **7**(2), 29 (2011).
- [39] D. U. Onah, C. E. Okeke, F. I. Ezema, Asian Transactions on Science and Technology **2**(1), 32 (2012)..
- [40] P. E Agbo, G. F. Ibeh, S. O. Okeke, J. E. Epke, Communications in Applied Sciences **1**(1), 38 (2013).
- [41] K. S. Dhirendra, Role of CdSe/ZnS Quantum Dots in Controlling Field Dependent Carrier Mobility in Polyflourene. 17th International Workshop on the Physics of Semiconductor devices, Amity Institute of Advanced Research and Studies (Material & Devices), Amity University Uttar Pradesh, India, (2013).
- [42] S. Simrjit, Enhanced Photocatalysis in CdS/ZnO Core/Shell nanostructures. 17th

- International Workshop on the Physics of Semiconductor devices, Amity Institute of Advanced Research and Studies (Material & Devices), Amity University Uttar Pradesh, India, (2013).
- [43] M. Kavitha, M. Saroja, V. K. Romesh, G. Jenifer, International Journal of Thin Films Science and Technology **5**(2), 137 (2016).
- [44] M. Habib ,Y. K. Woo, D. J. Kwang , J. J. Oh-Shim, Applied surfaces Science, (2005) 72-76.
- [45] K. O. Ovid, Rev. Adv. Mater. Sci. **1**, 61 (2000).
- [46] K. L. Chopra, Thin Film Phenomena MC Graw Hill Co., New York, USA, (1969).
- [47] L. I. Maissel, R. Glang, (eds) Hand book of Thin Film technology, MC Graw Hill Co., New York, USA, (1970).
- [48] O. Mustafa, Chin. Phys. Lett, 25 (2008).
- [49] Lambert-Beer's law Source: <http://www.wikilectures.eu/index-php?oldid-24362>.
- [50] A. I. Onyia, M. N. Nnabuchi, Study of Optical properties of CdS/PbS and PbS/CdS Heterojunction Thin Films Deposited using Solution Growth Technique, Proceedings of the 1st African International Conference/Workshop on Applications of Nanotechnology to Energy, Health and Environment, UNN, March 23 – 29, (2014).
- [51] S. Manouchehri, J. Zahmatkesh, M. Heidari-Sani, T. Barzekar, M. H. Yousefi, Experiment, **26**(3) 1816 (2014).
- [52] M. Born, E. Wolf, Principle of Optics, Pergamon Oxford, 24-60 (1989).
- [53] V. Maurice, T. Georgelin, J. M. Siaugue, V. Cabuil, Magn. Mater. **321**, 1408 (2009).
- [54] S. R. Chopra, Thin Film Solar cells, Plenum New York, 118 (1983).
- [55] K. S. Chou, C. C. Chen, Mesopor. Mater. **98**, 2008(2007).